

Spin-Resolved Resonant Electron Energy-Loss Spectroscopy (SR-rEELS): Observation of Element- and Spin-Selective Bulk Plasmons

Shin-ichi Kimura,^{1,2,3,*} Taishi Kawabata,² Hiroki Matsumoto,² Yu Ohta,² Ayuki Yoshizumi,² Yuto Yoshida,²
Takumi Yamashita,² Hiroshi Watanabe,^{1,2} Yoshiyuki Ohtsubo,^{1,2} Naoto Yamamoto,⁴ and Xiuguang Jin⁴

¹*Graduate School of Frontier Biosciences, Osaka University, Suita, Osaka 565-0871, Japan*

²*Department of Physics, Graduate School of Science,
Osaka University, Toyonaka, Osaka 560-0043, Japan*

³*Institute for Molecular Science, Okazaki, Aichi 444-8585, Japan*

⁴*High Energy Accelerator Research Organization (KEK), Tsukuba, Ibaraki 305-0801, Japan*

(Dated: January 18, 2022)

We have developed spin-resolved resonant electron energy-loss spectroscopy (SR-rEELS) in the primary energy of 0.3–1.5 keV, which corresponds to the core excitations of $2p \rightarrow 3d$ absorption of transition metals and $3d \rightarrow 4f$ absorption of rare earths. Element-specific carrier and valence plasmons can be observed by using the resonance enhancement of core absorptions. Spin-resolved plasmons were also observed using a spin-polarized electron source from a GaAs/GaAsP strained superlattice photocathode. Furthermore, this primary energy corresponds to an electron penetration depth of 1 to 10 nm and thus provides bulk-sensitive EELS spectra. The methodology is expected to complement the element-selective observation of elementary excitations by resonant inelastic x-ray scattering and resonant photoelectron spectroscopy.

I. INTRODUCTION

In recent years, resonant PhotoElectron Spectroscopy (rPES) and Resonant Inelastic X-ray Scattering (RIXS) using synchrotron radiation have been widely used to observe elementary excitations of interacting electrons, so-called quasiparticles, and collective excitations such as magnons and plasmons in an element-selective manner [1]. These methods have been successful in observing physical quantities that cannot be measured by other methods, such as the direct observation of the hybridization bands between conduction and localized $4f$ states in rare-earth compounds [2] and magnon dispersions in high- T_c cuprate superconductors [3]. The optical process of rPES and RIXS are described in Figs. 1(a) and 1(c), respectively. Complementary to these techniques are resonant Inverse PhotoElectron Spectroscopy [rIPES, Fig. 1(b)], which is the inverse process of rPES, and resonant Electron Energy-Loss Spectroscopy [rEELS, Fig. 1(d)], which is the inelastic scattering of electron beams, i.e., the sample is resonantly excited by a monochromatic electron beam that matches the energy of inner-shell absorptions. These resonant high-energy spectroscopies are complementary methods to one another. Among these methods, rEELS with the primary energy (E_i) of 0.4–1.6 keV, where the absorptions of transition metals' $2p \rightarrow 3d$ and rare earths' $3d \rightarrow 4f$ transitions are located, has not been performed yet. While rIPES and rEELS have the advantage of the capability of element-selective measurements, they cannot achieve high energy resolution. The reason is that it is difficult to change the energy while maintaining high energy resolution and high flux with commonly used thermal electron

sources. For example, the energy resolution of rIPES is about 0.5 eV [4], and that of EELS at $E_i \sim 1$ keV is currently about 0.25 eV [5]. These energy resolutions are not very high compared to the current standard resolutions of rPES (~ 10 meV in the vacuum-ultraviolet region [6] and ~ 100 meV in the soft-x-ray region [7]) and RIXS (~ 100 meV) [8].

High-Resolution EELS (HR-EELS) using low-energy electron beams of 100 eV or less with the energy resolution of less than several tens of meV is widely used as a method for observing the $E - \vec{q}$ curve (\vec{q} is the relative momentum transfer) of collective excitations such as plasmons and phonons in materials, which is complementary to Angle-Resolved PhotoElectron Spectroscopy (ARPES), in which band structures and quasiparticle dispersion ($E - \vec{k}$ curve, \vec{k} is the momentum) are observed [9]. The other is TEM-EELS, which uses high-energy electron beams of several tens of keV or higher using a transmission electron microscope [10]. Among these present EELS measurements, HR-EELS is mainly used to observe surface phonons due to the surface sensitivity of low-energy electron beams. On the other hand, TEM-EELS is used to measure the transmitted EELS of ultra-thin samples and has the advantage of obtaining bulk information in a small area by using an electron microscope. However, with a few exceptions [11], TEM-EELS has no high energy resolution (~ 0.2 eV) [12], and since the electron beam energy is fixed, it is difficult to make element-specific measurements by resonance. Also, it is difficult to observe the spectra by selecting the electron spin direction.

To observe element-specific, spin-resolved elementary excitations in solids, we have developed Spin-Resolved rEELS (SR-rEELS) with $E_i = 0.3 - 1.5$ keV to complement the EELS methods described above and obtain complementary information to RIXS using synchrotron

* kimura@fbs.osaka-u.ac.jp

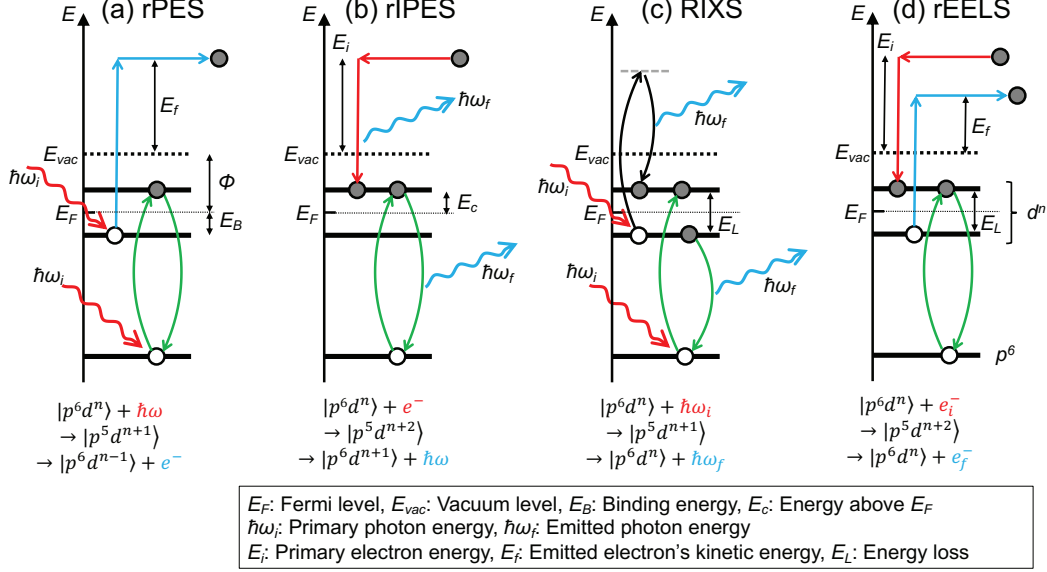


FIG. 1. Resonant high-energy spectroscopies using synchrotron radiation and monochromatized electron source, (a) resonant PhotoElectron Spectroscopy (rPES), (b) resonant Inverse PhotoElectron Spectroscopy (rIPES), (c) Resonant Inelastic X-ray Scattering (RIXS), and (d) resonant inelastic electron scattering, namely resonant Electron Energy-Loss Spectroscopy (rEELS). This is the example of the resonance of the $2p$ - $3d$ absorption edge of transition-metal compounds, in the case of rare-earth compounds, the absorption process should be changed to the $3d$ - $4f$ absorption. These methods provide us complementary information of quasiparticles and collective excitations of matter.

radiation. In SR-rEELS, the negative electron affinity (NEA) surface of a GaAs/GaAsP strained superlattice is used as a photocathode electron source [13], and the spin-polarized electron beam extracted from the NEA surface is irradiated to samples with kinetic energies of 0.3–1.5 keV. The inelastically scattered electrons are observed by a photoelectron analyzer. The energy width of the electron beam is $2\sigma \sim 100$ meV, which is considered sufficient for plasmon measurement. Therefore, it is possible to construct an rEELS system without a monochromator, and the ability to easily change the primary energy provides elemental selectivity based on resonance effects. Besides, the electrons at this energy have a mean free path of a few nm [14], so they are highly bulk sensitive and can provide information on bulk plasmons. Furthermore, the spin polarization of the electron beam is more than 80 % in the GaAs/GaAsP strained superlattice used as an electron source [15], compared to 50 % in ordinary bulk GaAs [16], which enables highly accurate spin polarization measurements.

In this paper, we report the outline of the SR-rEELS system developed here. First, a description of the system is given, followed by the characteristics of the electron source and its energy resolution. After that, we show the EELS spectra of Au and Ag as typical examples and compare them with the bulk loss function spectra obtained from the optical reflectivity spectra. Furthermore, resonance effects are introduced, such as the Ni $2p$ - $3d$ resonance enhancement of the charge-transfer and d - d ex-

citations of a transition-metal compound NiO and the $3d$ - $4f$ resonance of a rare-earth compound SmB₆ in carrier plasmon. Finally, the spin-resolved EELS spectra of Fe thin films are presented.

II. SPIN-RESOLVED RESONANT ELECTRON-ENERGY-LOSS SPECTROSCOPY (SR-rEELS) APPARATUS

Figure 2 shows an overview and a cross-sectional view of the SR-rEELS apparatus and the electron beam path. The SR-rEELS apparatus is a combination of a photoelectron spectrometer and a spin-polarized electron source.

The photoelectron spectrometer is a hemispherical analyzer (SES100, VG-Scienta AB) with an orbital radius of 100 mm. A helium discharge lamp with a monochromator (VUV5000, VUV5040, VG-Scienta AB) and an x-ray tube (XR-50, SPECS GmbH) are used as the UV light source and an x-ray source, respectively, to compare the quasiparticle electronic structure with obtained EELS spectra and check the surface conditions by the UV-ARPES and x-ray photoelectron spectroscopy.

The spin-polarized electron source is a photocathode based on two kinds of GaAs/GaAsP strained superlattice [17]: One is a 12-pair strain-compensated superlattice (SCSL), and the other a 12-pair strained superlattice (SSL) [18]. The NEA surface is created by depositing Cs

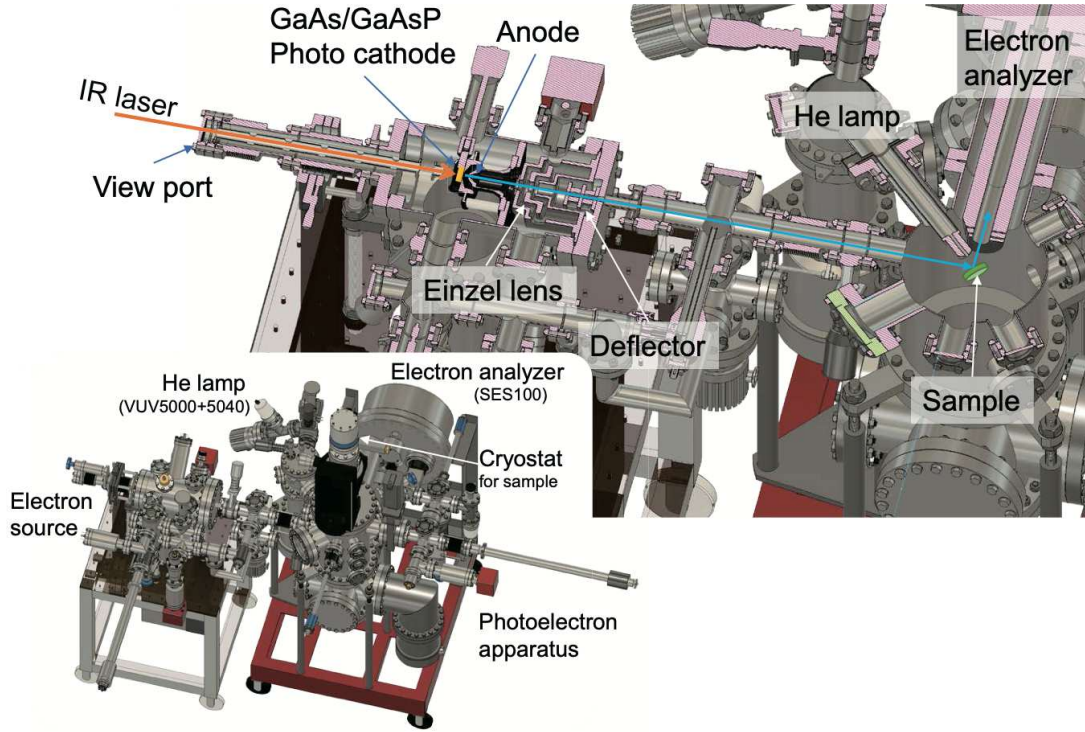


FIG. 2. Spin-Resolved resonant Electron Energy-Loss Spectroscopy (SR-rEELS) setup. The overview of the SR-rEELS apparatus, which includes spin-polarized electron source and photoelectron spectroscopy setup, is shown in the lower figure, and the electron path of the incident and scattered electrons with the IR laser of the excitation to the photocathode in the cross-sectional view of the setup is also shown in the upper figure. The photoelectron setup equips a hemispherical electron analyzer (SES100) and two light source, a He lamp with a monochromator (VUV5000+5040) and an x-ray tube (XR-50, not shown in the figure).

on the GaAs surface. An IR laser of 785 nm wavelength is irradiated from the backside through the GaP substrate to the GaAs surface to emit electrons [13]. The generated electron beam is focused on the sample surface by an Einzel lens and a deflector that adjusts the XY axis. This electron source is used for SR-rEELS and RHEED measurements of the same sample condition, so the photocathode is designed to be capable of applying up to -30 kV and the constant voltage supply with a extreme-high voltage accuracy of less than 1 ppm (IPES-30kV, MBScientific AB) is used for acceleration.

To obtain a spin-polarized electron beam, the incident linearly-polarized IR laser light is converted to left and right circular polarization using a $1/4\text{-}\lambda$ plate and irradiated to the photocathode. The sample is then irradiated with spin-polarized electron beams whose electron spins are parallel/antiparallel to the direction of the incident electrons.

We used electrons near the threshold energy of the NEA surface of GaAs, which is expected to be highly monochromatic, to irradiate the sample directly without passing through a monochromator. To evaluate the energy width of the electron beam, we firstly introduced the electron beam to the electron analyzer directly and measured the energy width by the observation of the spectral

distribution.

The inset in Fig. 3 is a typical spectrum showing the energy distribution of the electron beam from the electron source (the bias voltage of the photocathode is -1500 V, i.e., the kinetic energy of electrons $E_K = 1500$ eV). SSL has been used as the photocathode. The peak width was found to be 117 ± 10 meV for 2σ by fitting with Gaussian. The maximum electron flux was roughly evaluated as about 10^{12} s^{-1} at the laser power of about 100 mW. The measurement results for the bias voltage dependence of the photocathode, i.e., changing the kinetic energy, is shown in Fig. 3. From this figure, 2σ is 80–85 meV at $E_K = 300$ and 500 eV, and as E_K increases, 2σ increases. Here, the energy resolution of the electron analyzer was set as about 20 meV. So, the energy width of electron beam is about 77 meV (115 meV) at $E_K = 500$ eV (1500 eV). The minimum energy width at $E_K = 500$ eV is similar to that of the photoluminescence (PL) peak [18]. Since the PL peak of SCSL is sharper than that of SSL, the energy width of SCSL may become smaller than that shown in Fig. 3.

Although the energy width obtained here is not as narrow as that of HR-EELS [19] or very high-resolution TEM-EELS (about 10 meV) [20], the energy width is narrower than that previously reported, about 0.25 eV

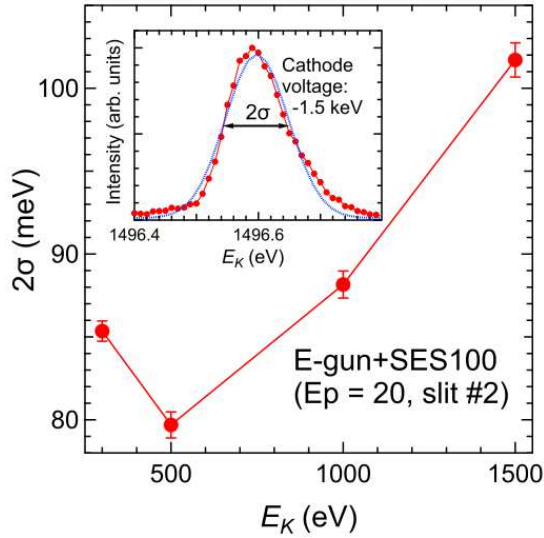


FIG. 3. Energy width (2σ) of the electron source shown in Fig. 2 as a function of kinetic energy. The electron-analyzer's energy resolution is set as about 20 meV by the pass energy E_p and slit number. Inset: A typical spectrum of the electron beam of $E_K = 1500$ eV from the electron source directly measured by the photoelectron analyzer.

and more at $E_i \sim 1$ keV [5, 21].

The obtained energy width is approximately equivalent to the room temperature energy width of $4k_B T \sim 0.1$ eV. In other words, thermal fluctuations of electrons in the photocathode are considered to be manifested. It has been reported that the energy width becomes narrower when the photocathode is cooled down [22]. Therefore, to further narrow the energy width, it is necessary to consider cooling the photocathode.

Also, since EELS can detect the same excitations as RIXS and the SR-rEELS apparatus has the similar energy resolution to soft-x-ray RIXS (SX-RIXS) beamlines [8, 23], SR-rEELS becomes a complementary method to the SX-RIXS. Furthermore, since SR-rEELS can characterize the spin-polarization of electrons, it can provide additional information of electron spins to the present SX-RIXS.

III. MEASUREMENT RESULTS

A. EELS on gold and silver films

In order to evaluate the constructed SR-rEELS system, the spectra of gold (Au) and silver (Ag) polycrystalline thin films were firstly measured and are shown in Fig. 4. In a previous study, the energy width of the primary electrons E_i was reported to be about 0.7 eV [25]. The resolution is not good enough to compare with the present study. Therefore, the loss function spectra $[Im(-\epsilon(\omega))^{-1}: \text{LF}]$ derived from the optical reflectivity

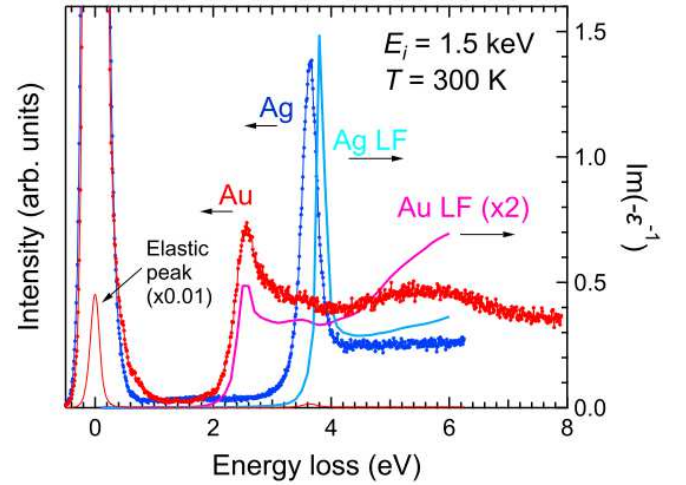


FIG. 4. EELS spectra of gold (Au) and silver (Ag) films with the primary energy $E_i = 1500$ eV at the temperature of 300 K accompanied with the corresponding loss function (LF) spectra obtained by the Kramers-Kronig analysis of the optical reflectivity spectra [24].

spectra [24] are also shown here together. In the EELS spectrum of Au, carrier plasmon peaks at the energy loss $E_L \sim 2.5$ eV and valence plasmon peaks at $E_L \sim 3.5$ eV and 5.5 eV were visible. Among these peaks, the peaks at $E_L \sim 2.5$ eV and 3.5 eV are in good agreement with the LF spectrum. The 5.5 eV peak is at the highest energy of the LF spectrum and is difficult to evaluate quantitatively. The LF spectrum reflects the bulk information obtained in the optical reflectivity spectrum, i.e., it can be regarded as a bulk plasmon spectrum. Therefore, the EELS spectrum is also considered to reflect the bulk plasmons. This result can be considered as a benefit of using the bulk-sensitive 1.5-keV electron beam.

The EELS spectrum of the Ag film, on the other hand, shows a carrier plasmon peak at $E_L \sim 3.6$ eV. In the LF spectrum, the corresponding peak is located at a slightly higher energy of $E_L \sim 3.8$ eV. This peak may originate from a surface plasmon located at slightly lower energy than that of the bulk plasmon of Ag [26]. Furthermore, this EELS peak is broader than that of the LF peak. The end of the peak (the kink of the spectrum) at about 4 eV is consistent with that of the LF peak, so the bulk plasmon peak seems to overlap at the high energy side. Since the HR-EELS spectrum only has a narrow surface plasmon peak [27], our EELS can be regarded to include not only the surface component but also the bulk component, i.e., we can confirm again that the EELS with $E_i = 1.5$ keV is a bulk-sensitive measurement.

B. rEELS on a transition-metal compound NiO

To check the resonance effect in the EELS measurement, the primary energy dependence of the EELS spec-

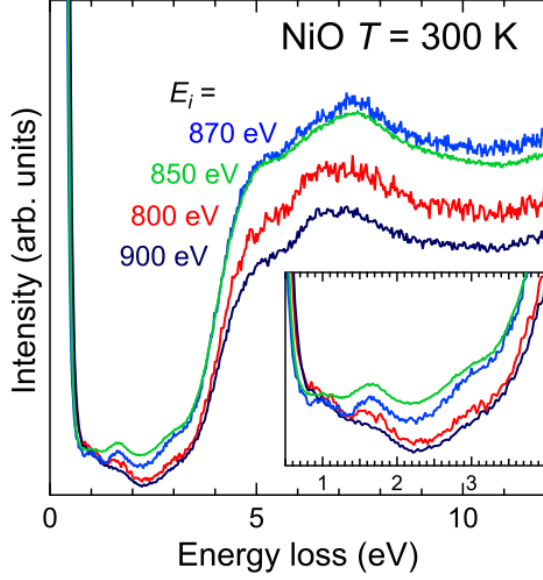


FIG. 5. Resonant EELS spectra of nickel monoxide NiO with the primary energies (E_i) of 800–900 eV. The overall spectral intensity is enhanced at $E_i = 850$ and 870 eV near the Ni $2d$ absorption edge. (Inset) Enlarged view of the Ni $d-d$ excitation area below the lowest charge transfer excitation energy of about 4 eV. The Ni $d-d$ excitations are also enhanced.

tra of nickel monoxide (NiO), which has several previous SR-EELS studies with E_i less than 100 eV [5, 28–30], has been investigated. The rEELS spectra at $E_i = 800 - 900$ eV near the Ni $2p \rightarrow 3d$ absorption edge are shown in Fig. 5. These spectra were normalized at the intensity of the elastic peak. The main structure in the energy region above 4 eV originates from the charge transfer excitation from the hybridization band between the Ni $3d$ lower-Hubbard band and the O $2p$ state to the Ni $3d$ upper-Hubbard band [31–33]. Compared to the spectra at $E_i = 800$ eV and 900 eV, the spectral intensities at $E_i = 850$ eV and 870 eV increase. Since the energies of Ni $2p_{5/2}$ and $2p_{3/2}$ absorption edge are about 850 eV and 870 eV, respectively, the spectral intensity enhancements are considered to originate from a resonance effect. It should be noted that the enhancement ratio is not higher than that of the rPES at the $2p$ absorption edge [34]. The reason is not clear yet, but this observation of rEELS at the $2p$ absorption edge is the first time.

The inset shows the Ni $d-d$ excitation peaks below the charge-transfer gap at about 4 eV. Among these peaks, especially the peaks at $E_L \sim 1.7$ eV and 3.0 eV are resonantly enhanced. This result is also in good agreement with the rEELS result [35] for the Ni $3s$ -edge (~ 100 eV). In the optical absorption spectrum, there are no peaks in this energy range [31] because the $d-d$ excitation is not a dipole-allowed transition. Therefore, the rEELS spectra can provide additional information to optical spectra.

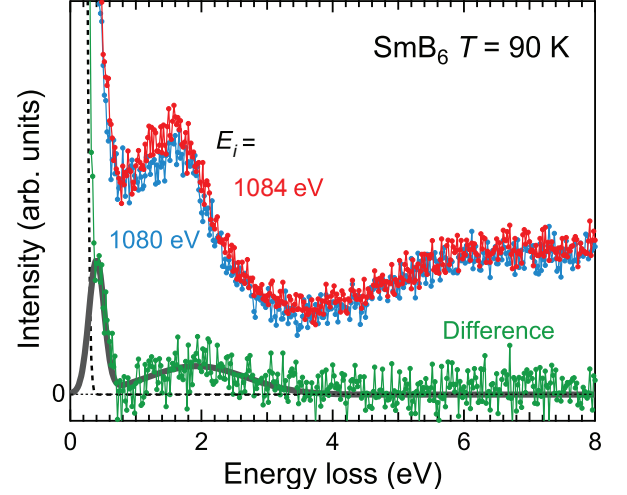


FIG. 6. EELS spectra of SmB₆ with the primary energies E_i of 1080 and 1084 eV and the difference spectrum $[I(E_L, E_i = 1084 \text{ eV}) - I(E_L, E_i = 1080 \text{ eV})]$. The dashed line is a Gaussian fitting curve to the difference spectrum of the elastic peaks of different primary energies. The solid line is a fitting curve with two Gaussians after subtraction the dashed line from the difference spectrum. The lower-energy peak at about 0.4 eV and the higher-energy peak at about 2 eV are considered to originate from the $4f$ - $5d$ interband transition and the carrier plasmon, respectively.

C. rEELS on a rare-earth compound SmB₆

Resonances of charge transfer and $d-d$ excitations were observed in NiO. The resonances are due to the Ni orbitals localized near the nucleus, so, naturally, they are observed. Next, we investigated whether or not carrier plasmon, which is less localized, resonates. The sample was samarium hexaboride (SmB₆), which has recently attracted attention as a topological Kondo insulator [36–40]. This carrier is based on the Sm $5d$ band and is expected to resonate at the Sm $3d$ absorption edge ($E_i \sim 1080$ – 1090 eV). Figure 6 shows the EELS spectra at $E_i = 1080$ eV and 1084 eV. Peaks at $E_L \sim 2$ eV and 6 eV are observed in the spectra. The former peak corresponds to the plasma edge (bulk plasmon) of the optical reflectivity spectrum [41], and the latter corresponds to the electronic excitation in the boron $2s$ and $2p$ orbitals [42]. There seems to be almost no difference between spectra of $E_i = 1080$ eV and 1084 eV, but a slight difference appears below 3 eV in the difference spectrum. The carrier plasmon peak at $E_L \sim 2$ eV has an intensity in the difference spectrum, but no structure appears at $E_L \sim 6$ eV. This result may indicate that the carrier plasmon is resonantly enhanced at the Sm $3d$ absorption edge, that is, the carrier originates from Sm site as the reasonable reason. The difference spectrum has a large upturn below 0.4 eV, which may originate from a slight difference between the elastic peaks of the different pri-

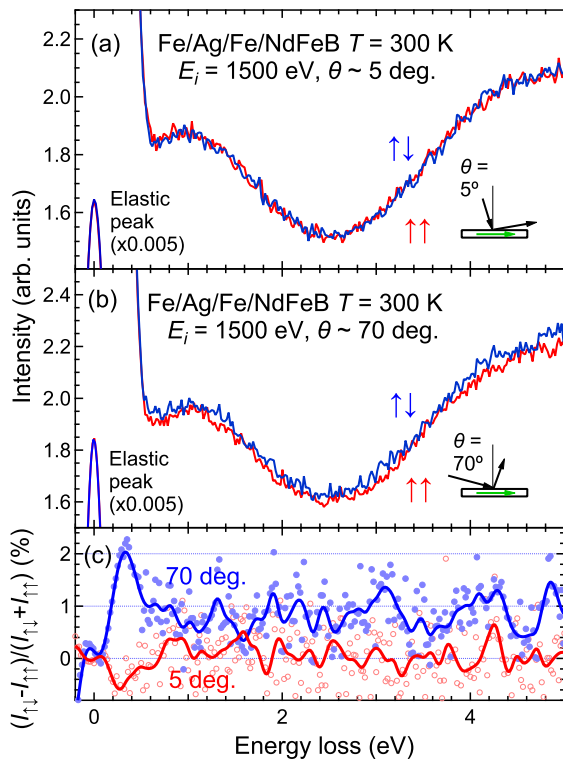


FIG. 7. Spin-resolved EELS spectra of a magnetized iron (Fe) film taken at the incident angles of 5 deg. (a) and 70 deg. (b) from the sample normal direction, and their spin asymmetry $[(I_{\uparrow\downarrow} - I_{\uparrow\uparrow}) / (I_{\uparrow\downarrow} + I_{\uparrow\uparrow})]$ spectra (c). The spin asymmetry spectra (solid circles for 70 deg. and open circles for 5 deg.) are very noisy owing to the very low inelastic scattering intensities, so the spectra are smoothed by averaging every ten points as shown by solid lines.

mary energies. After subtracting the upturn by a Gaussian fitting function, two peaks are visible below 4 eV. The lower-energy peak with the center at about 0.4 eV is larger than that at about 2 eV. In the energy region at around 0.4 eV, the $\text{Sm } 4f \rightarrow 5d$ interband transition has been observed in the optical conductivity spectrum [41]. Therefore, this is reasonable evidence that the resonant enhancement of the spatially expanded carrier plasmon is smaller than that of the localized interband transition. Combining with the result of NiO, it is suggested that the enhancement rate by resonance is related to the localization of electrons.

D. SR-EELS on iron film

Finally, the SR-EELS results using a magnetized Fe thin film are shown in Fig. 7. For this sample, a Fe substrate with a size of about $2 \times 2 \times 0.1 \text{ mm}^3$ was attached on top of a Nd-Fe-B magnet ($\sim 1 \times 1 \times 1 \text{ mm}^3$). The direction of magnetization was set parallel to the substrate

surface in the incident plane. The magnitude of the magnetization at the substrate surface was about 10^{-4} T. The silver polycrystalline thin film with the thickness of a few tens of nm was deposited on this substrate as a buffer layer, and a few nm of Fe polycrystalline film was deposited on top of it. The vacuum during the deposition was less than 1×10^{-6} Pa. The Fe film is not a single crystal, but we believe that this is not a problem because the purpose here is to observe the change in SR-EELS spectra due to the difference of the scattering intensity of spin-polarized electrons by the magnetization direction. The spin-polarized electrons were obtained by injecting a left-right circularly polarized IR laser beam into a photocathode with a $1/4\text{-}\lambda$ plate tilted by ± 45 deg. from the linear polarization plane. Then the spin direction of primary electrons is parallel or antiparallel to the electron beam direction.

Figure 7 compares the spectra of the incident electron spin parallel ($\uparrow\uparrow$) and antiparallel ($\uparrow\downarrow$) to the magnetization direction when the angle between the incident electron beam and the surface perpendicular is set to a near-normal incidence of 5 deg. (Fig. 7(a)) and a grazing incidence of 70 deg. (Fig. 7(b)) from the normal direction of the sample surface. The spectra are normalized at the elastic peak intensity. In the near-normal incidence configuration of Fig. 7(a), almost identical spectra were obtained for the two combinations. This result is because the directions of the incident electron spin and the magnetization are almost orthogonal, and there is little change even when the electron spin direction is changed. On the other hand, in Fig. 7(b), the incident electron spin direction is almost parallel to the magnetization direction. In this configuration, the intensity of $\uparrow\downarrow$ is higher than that of $\uparrow\uparrow$ at $E_L \geq 0.5$ eV, where the elastic peak's tail does not affect. The spin asymmetry $[(I_{\uparrow\downarrow} - I_{\uparrow\uparrow}) / (I_{\uparrow\downarrow} + I_{\uparrow\uparrow})]$ spectra of different incident angles are shown in Fig. 7(c). The spectrum of the near-normal incidence is almost zero in the energy region above 0.5 eV. In contrast, the spectrum of the grazing incidence has a spin asymmetry of about 1 % in the whole region. After smoothing the spin asymmetry spectra, some peaks at $E_L \sim 1.4, 2.0, 3.1$, and 4.3 eV are visible. This result is almost consistent with that of a previous SR-EELS spectrum for 20 ML bcc-Fe/Ag(100) [43] and Fe/W(110) [44]. Therefore, our SR-EELS can provide plausible information on the spin-polarization of materials.

IV. CONCLUSION

We have developed spin-resolved resonant electron energy-loss spectroscopy (SR-rEELS) at the transition metals' $2p$ - and rare earths' $3d$ -absorption edges. The current energy resolution is about 100 meV or less, and it is found that the charge-transfer and d - d excitations of NiO and the carrier plasmon and the $4f$ - $5d$ absorption of SmB_6 have apparent resonance effects. Furthermore, spin-dependent EELS spectrum parallel and antiparallel

to the direction of the electron beam were observed in a magnetized Fe film. The apparatus developed here will be helpful to clarify the nature of spin currents, which are essential for spintronics.

ACKNOWLEDGMENTS

We would like to thank Prof. Iga for providing high quality SmB₆ samples. This work was partly supported by JSPS KAKENHI (Grant Nos. 15H03676, 20H04453), and The Research Grants of Mitsubishi Foundation, The Murata Science Foundation, and The Research Foundation for Opto-Science and Technology.

-
- [1] L. J. Ament, M. Van Veenendaal, T. P. Devereaux, J. P. Hill, and J. Van Den Brink, *Rev. Mod. Phys.* **83**, 705 (2011), arXiv:1009.3630.
 - [2] H. J. Im, T. Ito, H.-D. Kim, S. Kimura, K. E. Lee, J. B. Hong, Y. S. Kwon, A. Yasui, and H. Yamagami, *Phys. Rev. Lett.* **100**, 176402 (2008).
 - [3] K. Ishii, S. Asano, M. Ashida, M. Fujita, B. Yu, M. Greven, J. Okamoto, D.-J. Huang, and J. Mizuki, *Phys. Rev. Mater.* **5**, 024803 (2021).
 - [4] Y. Tezuka and S. Shin, *J. Electron Spectros. Relat. Phenomena* **136**, 151 (2004).
 - [5] A. Gorschl ter and H. Merz, *Phys. Rev. B* **49**, 17293 (1994).
 - [6] S.-I. Kimura, T. Ito, M. Sakai, E. Nakamura, N. Kondo, T. Horigome, K. Hayashi, M. Hosaka, M. Katoh, T. Goto, T. Ejima, and K. Soda, *Rev. Sci. Instrum.* **81**, 053104 (2010).
 - [7] M. Y. Kimura, K. Fukushima, H. Takeuchi, S. Ikeda, H. Sugiyama, Y. Tomida, G. Kuwahara, H. Fujiwara, T. Kiss, A. Yasui, I. Kawasaki, H. Yamagami, Y. Saitoh, T. Muro, T. Ebihara, and A. Sekiyama, *J. Phys. Conf. Ser.* **592**, 012003 (2015).
 - [8] V. N. Strocov, T. Schmitt, U. Flechsig, T. Schmidt, A. Imhof, Q. Chen, J. Raabe, R. Betemps, D. Zimoch, J. Krempasky, X. Wang, M. Grioni, A. Piazzalunga, and L. Patthey, *J. Synchrotron Radiat.* **17**, 631 (2010), arXiv:0911.2598.
 - [9] S. Vig, A. Kogar, M. Mitrano, A. Husain, L. Venema, M. Rak, V. Mishra, P. Johnson, G. Gu, E. Fradkin, M. Norman, and P. Abbamonte, *SciPost Phys.* **3**, 026 (2017).
 - [10] F. Hofer, F. P. Schmidt, W. Grogger, and G. Kothleitner, *IOP Conf. Ser. Mater. Sci. Eng.* **109**, 012007 (2016).
 - [11] O. Krivanek, N. Dellby, J. Hachtel, J.-C. Idrobo, M. Hotz, B. Plotkin-Swing, N. Bacon, A. Bleloch, G. Corbin, M. Hoffman, C. Meyer, and T. Lovejoy, *Ultramicroscopy* **203**, 60 (2019).
 - [12] W. Grogger, F. Hofer, G. Kothleitner, and B. Schaffer, *Top. Catal.* **50**, 200 (2008).
 - [13] N. Yamamoto, T. Nakanishi, A. Mano, Y. Nakagawa, S. Okumi, M. Yamamoto, T. Konomi, X. Jin, T. Ujihara, Y. Takeda, T. Ohshima, T. Saka, T. Kato, H. Hori-naka, T. Yasue, T. Koshikawa, and M. Kuwahara, *J. Appl. Phys.* **103**, 064905 (2008).
 - [14] A. Zangwill, *Phys. Surfaces* (Cambridge University Press, 1988).
 - [15] T. Saka, T. Kato, T. Nakanishi, S. Okumi, K. Togawa, H. Horinaka, T. Matsuyama, and T. Baba, *Surf. Sci.* **454-456**, 1042 (2000).
 - [16] D. T. Pierce, R. J. Celotta, G. C. Wang, W. N. Unertl, A. Galejs, C. E. Kuyatt, and S. R. Mielczarek, *Rev. Sci. Instrum.* **51**, 478 (1980).
 - [17] X. Jin, N. Yamamoto, Y. Nakagawa, A. Mano, T. Kato, M. Tanioku, T. Ujihara, Y. Takeda, S. Okumi, M. Yamamoto, T. Nakanishi, T. Saka, H. Hori-naka, T. Kato, T. Yasue, and T. Koshikawa, *Appl. Phys. Express* **1**, 045002 (2008).
 - [18] X. Jin, A. Mano, F. Ichihashi, N. Yamamoto, and Y. Takeda, *Appl. Phys. Express* **6**, 015801 (2013).
 - [19] H. Ibach, F. C. Bocquet, J. Sforzini, S. Soubatch, and F. S. Tautz, *Rev. Sci. Instrum.* **88**, 033903 (2017).
 - [20] O. L. Krivanek, T. C. Lovejoy, M. F. Murfitt, G. Skone, P. E. Batson, and N. Dellby, *J. Phys. Conf. Ser.* **522**, 012023 (2014).
 - [21] Z. Lounis, M. Bouslama, N. Berrouachedi, C. Jardin, L. Auvray, A. Abdellaoui, A. Ouerdane, and M. Ghaf-four, *Vacuum* **82**, 529 (2008).
 - [22] S. Pastuszka, M. Hoppe, D. Kratzmann, D. Schwalm, A. Wolf, A. S. Jaroshevich, S. N. Kosolobov, D. A. Orlov, and A. S. Terekhov, *J. Appl. Phys.* **88**, 6788 (2000).
 - [23] Y. Harada, M. Kobayashi, H. Niwa, Y. Senba, H. Ohashi, T. Tokushima, Y. Horikawa, S. Shin, and M. Oshima, *Rev. Sci. Instrum.* **83**, 013116 (2012).
 - [24] S. Babar and J. H. Weaver, *Appl. Opt.* **54**, 477 (2015).
 - [25] J. C. Ingram, K. W. Nebesny, and J. E. Pemberton, *Appl. Surf. Sci.* **44**, 293 (1990).
 - [26] S. Suto, K.-D. Tsuei, E. W. Plummer, and E. Burstein, *Phys. Rev. Lett.* **63**, 2590 (1989).
 - [27] M. Rocca and U. Valbusa, *Phys. Rev. Lett.* **64**, 2398 (1990).
 - [28] B. Fromme, C. Koch, R. Deussen, and E. Kisker, *Phys. Rev. Lett.* **75**, 693 (1995).
 - [29] P. Jones, J. E. Inglesfield, J. J. M. Michiels, C. J. Noble, V. M. Burke, and P. G. Burke, *Phys. Rev. B* **62**, 13508 (2000).
 - [30] B. Fromme, M. Schmitt, E. Kisker, A. Gorschl ter, and H. Merz, *Phys. Rev. B* **50**, 1874 (1994).
 - [31] R. J. Powell and W. E. Spicer, *Phys. Rev. B* **2**, 2182 (1970).
 - [32] G. A. Sawatzky and J. W. Allen, *Phys. Rev. Lett.* **53**, 2339 (1984).
 - [33] S. H fner and T. Riesterer, *Phys. Rev. B* **33**, 7267 (1986).
 - [34] O. Tjernberg, S. S derholm, U. Karlsson, G. Chiai, M. Qvarford, H. N yl n, and I. Lindau, *Phys. Rev. B - Condens. Matter Mater. Phys.* **53**, 10372 (1996).
 - [35] A. Gorschl ter and H. Merz, *J. Electron Spectros. Relat. Phenomena* **87**, 211 (1998).
 - [36] L. Li, K. Sun, C. Kurdak, and J. W. Allen, *Nat. Rev. Phys.* **2**, 463 (2020).
 - [37] M. Dzero, K. Sun, V. Galitski, and P. Coleman, *Phys. Rev. Lett.* **104**, 106408 (2010), arXiv:0912.3750.

- [38] M. Dzero, J. Xia, V. Galitski, and P. Coleman, *Annu. Rev. Condens. Matter Phys.* **7**, 249 (2016), arXiv:1711.07976.
- [39] H. Miyazaki, T. Hajiri, T. Ito, S. Kunii, and S.-i. Kimura, *Phys. Rev. B* **86**, 075105 (2012).
- [40] Y. Ohtsubo, Y. Yamashita, K. Hagiwara, S.-I. Ideta, K. Tanaka, R. Yukawa, K. Horiba, H. Kumigashira, K. Miyamoto, T. Okuda, W. Hirano, F. Iga, and S.-I. Kimura, *Nat. Commun.* **10**, 2298 (2019).
- [41] S.-i. Kimura, T. Nanba, S. Kunii, and T. Kasuya, *Phys. Rev. B* **50**, 1406 (1994).
- [42] S. Kimura, T. Nanba, M. Tomikawa, S. Kunii, and T. Kasuya, *Phys. Rev. B* **46**, 12196 (1992).
- [43] T. Komesu, G. D. Waddill, and J. G. Tobin, *J. Phys. Condens. Matter* **18**, 8829 (2006).
- [44] S. N. Samarin, O. M. Artamonov, A. P. Baraban, M. Kostylev, P. Guagliardo, and J. F. Williams, *Appl. Phys. Lett.* **107**, 101602 (2015).